Asymmetry in Platinum Acetylide Complexes: Confinement of the Triplet Exciton to the Lowest Energy Ligand

Thomas M. Cooper,*,† Douglas M. Krein,†,‡ Aaron R. Burke,†,‡ Daniel G. McLean,†,§ Joy E. Rogers,†,# and Jonathan E. Slagle†,+

Materials and Manufacturing Directorate, Air Force Research Laboratory, Wright-Patterson Air Force Base, Ohio 45433, Anteon Corporation, Dayton, Ohio 45431, SAIC, Dayton, Ohio 45434, UES, Inc., Dayton, Ohio 45432, and AT&T Corporation, Dayton, Ohio 45434

Received: August 23, 2006; In Final Form: October 11, 2006

To determine structure−optical property relationships in asymmetric platinum acetylide complexes, we synthesized the compounds *trans*-$Pt(PBu_3)_2(C{\equiv}CC_6H_5)(C{\equiv}C-C_6H_4-C{\equiv}CC_6H_5)$ (**PE1-2**), *trans*-$Pt(PBu_3)_2(C{\equiv}CC_6H_5)(C{\equiv}C-C_6H_4-C{\equiv}C-C_6H_4-C{\equiv}CC_6H_5)$ (**PE1-3**) and *trans*-$Pt(PBu_3)_2(C{\equiv}C-C_6H_4-C{\equiv}CC_6H_5)(C{\equiv}C-C_6H_4-C{\equiv}C-C_6H_4-C{\equiv}CC_6H_5)$ (**PE2-3**) that have different ligands on either side of the platinum and compared their spectroscopic properties to the symmetrical compounds **PE1**, **PE2** and **PE3**. We measured ground state absorption, fluorescence, phosphorescence and triplet state absorption spectra and performed density functional theory (DFT) calculations of frontier orbitals, lowest lying singlet states, triplet state geometries and energies. The absorption and emission spectra give evidence the singlet exciton is delocalized across the central platinum atom. The phosphorescence from the asymmetric complexes comes from the largest ligand. Time-dependent (TD) DFT calculations show the S_1 state has mostly highest occupied molecular orbital (HOMO) → lowest unoccupied molecular orbital (LUMO) character, with the LUMO delocalized over the chromophore. In the asymmetric chromophores, the LUMO resides on the larger ligand, suggesting the S_1 state has interligand charge transfer character. The triplet state geometries obtained from the DFT calculations show distortion on the lowest energy ligand, whereas the other ligand has the ground state geometry. The calculated trend in the triplet state energies agrees very well with the experimental trend. Calculations of triplet state spin density also show the triplet exciton is confined to one ligand. In the asymmetric complexes the spin density is confined to the largest ligand. The results show Kasha's rule applies to these complexes, where the triplet exciton moves to the lowest energy ligand.

Introduction

There has been considerable interest in the synthesis, spectroscopy, nonlinear optics and structure−property relationships of platinum acetylides.[1−7] They are exceptional systems for investigating triplet state phenomena like ground state absorption to the triplet state, intersystem crossing, and the triplet state absorption spectrum and phosphorescence.[8] In our laboratory, we have been investigating the relation between chemical structure and spectroscopic properties in platinum acetylide complexes.[1,9,10] We recently published a detailed investigation of the photophysical properties of a series of butadiynes having the formula $H-(C_6H_4-C{\equiv}C)_n-(C{\equiv}C-C_6H_4)_n-H$, $n = 1-3$, and ligands $H-(C_6H_4-C{\equiv}C)_n-H$, $n = 1-3$, and compared these to previous work done on a complimentary series of platinum-containing complexes having the formula *trans*-$Pt(P(C_4H_9)_3)_2((C{\equiv}C-C_6H_4)_n-H)_2$, $n = 1-3$.[1,11] More recently, we synthesized a series of half-platinum acetylide complexes having the formula *trans*-$Pt^{II}(PBu_3)_2((C{\equiv}CC_6H_4)_n-H)Cl$, $n = 1-3$.[12] In all these articles, analysis of the dependence of singlet and triplet state energies on chromophore length gives evidence that the singlet exciton is delocalized through the central platinum, whereas the triplet exciton is confined to one ligand.

Time-resolved infrared spectra of the triplet state *trans*-$Pt(PBu_3)_2((C{\equiv}C-C_6H_4-C{\equiv}CC_6H_5)_2$[13] give evidence the triplet state geometry has cumulene and quinone character. A related time-resolved infrared spectroscopy and theoretical study of *trans*-$Pt(PBu_3)_2(C{\equiv}CC_6H_5)_2$ gives evidence the triplet exciton is confined to one ligand.[6] Another theoretical study of the same compound also suggests the triplet state is confined to one ligand.[14] A suggested intersystem crossing mechanism in platinum acetylides involves an initial delocalized singlet state exciton converting to a triplet exciton confined to one ligand.

In this paper we describe the synthesis and characterization of three platinum acetylides *trans*-$Pt(PBu_3)_2(C{\equiv}CC_6H_5)(C{\equiv}C-C_6H_4-C{\equiv}CC_6H_5)$ (**PE1-2**), *trans*-$Pt(PBu_3)_2(C{\equiv}CC_6H_5)(C{\equiv}C-C_6H_4-C{\equiv}C-C_6H_4-C{\equiv}CC_6H_5)$ (**PE1-3**) and *trans*-$Pt(PBu_3)_2(C{\equiv}C-C_6H_4-C{\equiv}CC_6H_5)(C{\equiv}C-C_6H_4-C{\equiv}C-C_6H_4-C{\equiv}CC_6H_5)$ (**PE2-3**) that have different ligands on either side of the central platinum. These compounds have C_s symmetry and we compare their spectroscopic properties to the C_{2h} symmetry compounds **PE1**, **PE2** and **PE3**. The nomenclature is described in Figure 1. With the lower symmetry we can distinguish between two possible intersystem crossing mechanisms where the triplet exciton goes to either ligand or preferentially goes to one ligand. We found the singlet exciton to be delocalized throughout the molecule, and the triplet exciton to be confined

* To whom correspondence should be addressed. E-mail: Thomas.Cooper@wpafb.af.mil.
† Wright-Patterson Air Force Base.
‡ Anteon Corp.
§ SAIC.
# UES, Inc.
+ AT&T Corp.

10.1021/jp0654516 CCC: $33.50
Published on Web 11/30/2006

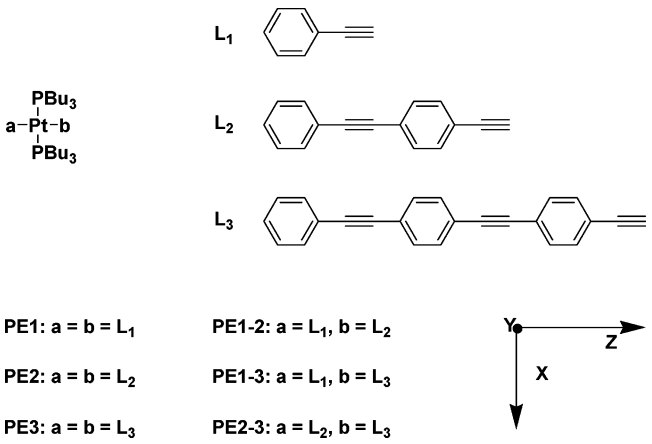

Figure 1. Chemical formulas and nomenclature. Arrows show molecular axes. Nomenclature for the asymmetric compound **a**-Pt$(PBu_3)_2$-**b**, designated as **PEa-b**, labels two ligands of the compound. In discussions below, ligand **a** is designated as the "left ligand" and ligand **b** is the "right ligand". When **a** = Cl, the chromophore is designated as "**half-PEb**". The butadiyne **PE*n***−C≡C−C≡C−**PE*n*** is labeled as "**PE*n*-BD**".

to the lowest energy ligand. We also did density functional theory (DFT) calculations on the ground and lowest triplet state of **PE1**, **PE2**, **PE3**, **PE1-2**, **PE1-3** and **PE2-3**. The experimental trends are reproduced very well by the DFT calculations.

General Synthesis Methods

All reactions were carried out using dry, distilled solvents and under dry, high purity nitrogen. All reagents were purchased from Aldrich Chemical Co. and used without further purification. Reverse phase column refers to Alltech Extract-Clean C18. The ligands **PE2-H** and **PE3-H** and compounds Pt(C≡C−C_6H_5)Cl$(PBu_3)_2$ (**half-PE1**), Pt(C≡C−C_6H_4−C≡C−C_6H_5)Cl-$(PBu_3)_2$ (**half-PE2**), Pt(C≡CC_6H_4C≡$CC_6H_5)_2(PBu_3)_2$ (**PE2**) and Pt(C≡CC_6H_4C≡CC_6H_4C≡$CC_6H_5)_2(PBu_3)_2$ (**PE3**) were synthesized as described previously.[1,12]

Synthesis

Pt(C≡CC_6H_5)(C≡CC_6H_4C≡CC_6H_5)$(PBu_3)_2$ (**PE1-2**) In a 100 mL three-neck round-bottom flask 480 mg (0.6535 mmol) of **half-PE1** was dissolved in 35 mL of diethylamine, followed by addition of 12.5 mg of CuI and 133 mg (0.6535 mmol) of **PE2-H.** The solution was heated to reflux and stirred overnight. The solvent was removed on a rotovap, and the remaining solid was then dissolved in dichloromethane (DCM) and adsorbed to a small amount of silica gel. This was layered over a 4 in. column of silica gel and eluted with first hexane and then varying percentages of a hexane/DCM mixture. Approximately 200 mg of the light yellow solid product was isolated. MA Found: C, 64.18; H, 7.36. $C_{48}H_{68}P_2Pt$ Requires: C, 63.91; H, 7.60. MW = 901. IR (KBr, thin film): 2099 cm^{-1} [ν(Pt−C≡C)]. ^{1}H NMR ($CDCl_3$): δ 0.96 (m, 18H, CH_3), 1.47 (m, 12H, CH_2), 1.60 (m, 12H, CH_2), 2.17 (m, 12H, CH_2), 7.25−7.40 ppm (m, 14H, ArH). ^{13}C NMR ($CDCl_3$): δ 14.09 (s, CH_3), 23.96 (t, J(CP) = 17 Hz, CH_2), 24.19 (t, J(CP) = 7 Hz, CH_2), 24.68 (t, J(CP) = 7 Hz, CH_2), 26.64 (s, CH_3), 108.0 (t, J(CP) = 14 Hz, Pt−C≡C), 112.4(t, J(CP) = 14 Hz. Pt−C≡C), 90.0 (s, C≡C), 90.4 (s, C≡C), 109.3 (s, C≡C), 109.4 (s, C≡C), 119.4, 123.9, 125.1, 128.1, 128.3, 128.6, 129.3, 129.5, 130.9, 131.0, 131.5, 131.7 ppm (Ar). ^{31}P NMR ($CDCl_3$): s and d centered at δ 4.25 ppm (J(PPt) = 2351 Hz, PBu_3). EIMS: m/z 901.

Pt(C≡CC_6H_5)(C≡CC_6H_4C≡CC_6H_4C≡CC_6H_5)$(PBu_3)_2$ (**PE1-3**) In a 100 mL three-neck round-bottom flask 418 mg (0.5721 mmol) of **half-PE1** was dissolved in 40 mL of diethylamine, followed by addition of 12.5 mg of CuI and 173 mg (0.5721 mmol) of **PE3-H**. The solution was heated to reflux and stirred overnight. The solvent was removed on a rotovap, and the remaining solid was then dissolved in DCM and adsorbed to a small amount of silica gel. This was layered over a 4 in. column of silica gel and eluted with first hexane and then varying percentages of a hexane/DCM mixture. Two fractions of the hexane/DCM eluents showed a mixture of product and **PE1** by NMR. These mixtures were combined and put through a 1 in. reversed phase column using acetonitrile and DCM as eluents. Approximately 130 mg of a waxy light yellow solid was isolated in an acetonitrile/DCM fraction. MA Found: C, 67.68; H, 6.90. $C_{56}H_{72}P_2Pt$ Requires: C, 67.11; H, 7.24. MW = 1001. IR (KBr, thin film): 2096 cm^{-1} [ν(Pt−C≡C)]. ^{1}H NMR ($CDCl_3$): δ 0.99 (m, 18H, CH_3), 1.49 (m, 12H, CH_2), 1.66 (m, 12H, CH_2), 2.19 (m, 12H, CH_2), 7.29−7.55 ppm (m, 18H, ArH). ^{13}C NMR ($CDCl_3$): δ 14.15 (s, CH_3), 24.19 (t, J(CP) = 17 Hz, CH_2), 24.64 (t, J(CP) = 7 Hz, CH_2), 24.82 (s, CH_2), 26.66, (s, CH3), 107.96 (t, J(CP) = 14 Hz, Pt−CC), 112.89 (t, J(CP) = 14 Hz, Pt−C≡C), 89.5 (s, C≡C), 89.9 (s, C≡C), 91.5 (s, C≡C), 92.4 (s, C≡C), 109.4 (s, C≡C), 109.5 (s, C≡C), 119.2, 123.1, 123.4, 123.7, 125.2, 128.2, 128.7 (br), 129.3, 129.7, 131.1 (br), 131.6, 131.7, 131.8, 131.9 ppm (Ar). ^{31}P NMR ($CDCl_3$): s and d centered at δ 4.26 ppm (J(PPt) = 2351 Hz, PBu_3). EIMS: m/z 1001.

Pt(C≡CC_6H_4C≡CC_6H_5)(C≡CC_6H_4C≡CC_6H_4C≡CC_6H_5)-$(PBu_3)_2$ (**PE2-3**) In a 100 mL three-neck round-bottom flask 546 mg (0.653 mmol) of **half-PE2** was dissolved in 50 mL of diethylamine, followed by addition of 12.5 mg of CuI and 157.5 mg (0.521 mmol) of **PE3-H**, and the mixture stirred for 4 days at room temperature. The solvent was removed on a Rotovap, and the remaining solid was then dissolved in DCM and occluded to a small amount of silica gel. This was layered over a 4 in. column of silica gel and eluted with first hexane and then varying percentages of a hexane/DCM mixture. The fraction eluted with a hexane/25% DCM mixture contained the product with a small amount of **half-PE2**. This fraction was put through a 1 in. reversed phase using methanol and varying MeOH/DCM mixtures as the eluent. Approximately 280 mg of a waxy light yellow solid was isolated from the MeOH/25% DCM fraction. MA Found: C, 69.71; H, 6.69. $C_{64}H_{76}P_2Pt$ Requires: C, 69.73; H, 6.95. MW = 1101. IR (KBr, thin film): 2095 cm^{-1} [ν(Pt−C≡C)]. ^{1}H NMR ($CDCl_3$): δ 0.97 (m, 18H, CH_3), 1.49 (m, 12H, CH_2), 1.66 (m, 12H, CH_2), 2.19 (m, 12H, CH_2), 7.26−7.60 (m, 22H, ArH) ppm. ^{13}C NMR ($CDCl_3$): δ 14.10 (s, CH_3), 24.47 (t, J(CP) = 17 Hz, CH_2), 24.69 (t, J(CP) = 17 Hz, CH_2), 26.65 (s, CH_3), 111.9 (t, J(CP) = 14 Hz, Pt−C≡C), 112.5 (t, J(CP) = 14 Hz, Pt−C≡C), 109.7 (s, br, C≡C), 89.5 (s, C≡C), 89.9 (s, C≡C), 90.1 (s, C≡C), 90.3 (s, C≡C), 91.4 (s, C≡C), 92.3 (s, C≡C), 119.2, 119.5, 123.1, 123.4, 123.7, 123.8, 128.3, 128.6, 128.79 (br), 129.4, 129.6, 131.0 (br), 131.50, 131.54, 131.65, 131.74, 131.8, 131.9 (Ar) ppm. ^{31}P NMR ($CDCl_3$): s and d centered at δ 4.34 (J(PPt) = 2351 Hz, PBu_3) ppm. EIMS: m/z 1101.

Computational Methods

Calculations were done using Gaussian 03W, revision D.01.[15] The presence of the heavy platinum center required a basis set that includes relativistic effects through an effective core potential. We used DFT with the B3LYP functional and the relativistic LANL2DZ basis set.[16,17] To save computer time, the phosphine portion of the molecule was converted from tributylphosphine to trimethylphosphine. We performed geometry

TABLE 1: Summary of ^{13}C NMR Data

compd	δ_a[a]	Δ_{ab}[b]	δ_b	Δ_{ba}	dipole moment[d]
PE1-2	108.0	−0.3	112.4	+0.4	1.153
PE1-3	108.0	−0.3	112.9	+0.5	1.627
PE2-3	111.9	−0.1	112.5	+0.1	0.458
PE1[c]	108.3				
PE2	112.0				
PE3	112.4				

[a] In the asymmetric **PEa-b** complexes, ligand **a** is the left ligand and ligand **b** is the right ligand. Chemical shifts are in ppm. [b] Change in chemical shift from reference symmetric complex. [c] Chemical shift values (δ_{aa}) for symmetric complexes obtained from the literature.[19] [d] Dipole moment (debye) calculated as described in the methods.

optimizations for the ground and T_1 states. For the ground state, energy minimizations were performed with the symmetrical complexes **PE*n*** having the ligand plane perpendicular to the P−Pt−P axis, constraining the symmetry to C_{2h} and the asymmetric complexes **PEa-b** to C_s. We used DFT to calculate the T_1 state geometry of the triplet state. DFT is known as a ground state theory only rigorously valid for the ground state of a given symmetry (including spin symmetry).[18] In this instance the T_1 state is the "ground state". Our starting geometry for these minimizations was that previously found for **PE1**,[14] where the ligand plane was parallel to the P−Pt−P axis and the symmetry allowed to be C_1. We used the ΔSCF method to estimate E_T as given by the expression

$$E_T = E(\text{triplet state relaxed geometry}) - E(\text{ground state relaxed geometry})$$

The singlet excited states were investigated by density functional response theory (TDDFT), where the 6 lowest singlet roots were obtained.

General Spectroscopy Techniques

All absorption and fluorescence spectra were obtained in benzene solutions. Ground state UV/vis absorption spectra were measured on a temperature-controlled Cary 500 spectrophotometer. Emission spectra at 5 nm slit width were measured using a Perkin-Elmer model LS 50B fluorometer. Low-temperature phosphorescence was done in methyltetrahydrofuran as a frozen glass at 77 K and exciting at 350 nm. Nanosecond transient absorption measurements were carried out using the third and fourth harmonics (355 and 266 nm) of a Q-switched Nd:YAG laser (Quantel Brilliant, pulse width ca. 5 ns). All samples were deoxygenated with three freeze−pump−thaw cycles. Pulse fluences of up to 8 mJ cm^{-2} are typically used at the excitation wavelength. Ground state absorption spectra were obtained before and after the flash photolysis experiment. Most samples showed less than 10% degradation. If necessary, spectra were collected from photosensitive samples by collecting the spectrum in a 100 nm increment and then putting a fresh sample into the instrument. A detailed description of the laser flash photolysis apparatus has been published.[1]

Results

Table 1 lists selected ^{13}C NMR data for the mixed compounds. The table lists the chemical shift for the Pt−C carbon. Also included are corresponding chemical shifts for the **PE*n*** complexes that have been previously published.[19] The magnitude of the shifts were similar to those seen in the symmetric complexes. For example, δ(**PE1-2**, ligand 1) ∼ δ(**PE1**) and δ(**PE1-2**, ligand 2) ∼ δ(**PE2**). The chemical shifts for the asymmetric complexes split into two values. For a complex

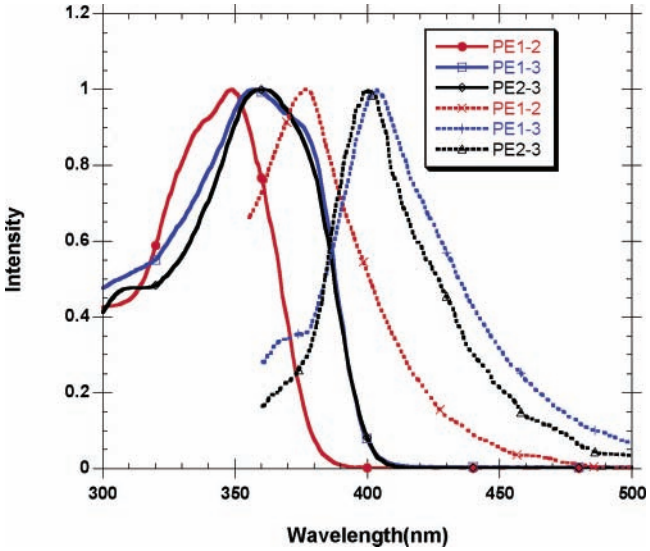

Figure 2. Ground state absorption and emission spectra of the complexes dissolved in benzene at room temperature. For the emission spectra, the excitation wavelength was 350 nm.

TABLE 2: Summary of Spectroscopic Data

compd	λ_{max}(GS)[a]	ϵ_{max}[a]	f[c]	λ_{max}(fl)[d]	λ_{max}(ph)[e]	λ_{max}(TT)[f]	τ(TT)[g]
PE1-2	349	57 665	1.34	377	524	590	93
PE1-3	357	69 414	1.97	403	555	650	144
PE2-3	359	101 815	2.74	401	553	650	16a

[a] Maximum of ground state absorption spectrum in benzene (nm). [b] Extinction coefficient ($M^{-1}cm^{-1}$). [c] Oscillator strength was obtained by fitting absorption spectrum to three Gaussians. [d] Maximum of fluorescence spectrum in benzene (nm). Excitation wavelength 355 nm. [e] Peak of 0−0 band of phosphorescence of complex in methyl-THF glass at 77 K. [f] Peak of triplet state absorption spectrum obtained from flash photolysis experiment. [g] Triplet state lifetime in μs.

PEab, the interaction between ligands **a** and **b** is determined by calculating the difference

$$\Delta_{ab} = \delta_a - \delta_{aa}$$

and

$$\Delta_{ba} = \delta_b - \delta_{bb}$$

where δ_a is the chemical shift of the Pt−C carbon of ligand **a** of the complex and δ_{aa} is the corresponding chemical shift for the complex **PEa**. Δ_{ab} is the influence of ligand **b** on ligand **a**. Similarly, the value Δ_{ba} is calculated from values for ligand **b** of the complex and the complex **PEb**. For a complex **PEa-b**, the interaction effect caused a small upfield shift in the left ligand **a** and a corresponding small downfield shift in the right ligand **b**. The magnitude of Δ behaves as **PE1-3** ∼ **PE1-2** > **PE2-3**. The dipole moment calculated by DFT follows a similar ordering: μ(**PE1-3**) > μ(**PE1-2**) > μ(**PE2-3**).

In Figure 2, the absorption spectrum of **PE1-2** has an absorption maximum of 349 nm, and that for **PE1-3** red-shifts to 357 nm. The band shape and absorption maximum of **PE2-3** are identical to those of **PE1-3**, although its spectrum has an increased extinction coefficient, as given in Table 2. All three absorption spectra have at least two closely spaced bands near the absorption maximum. A Gaussian fit of the spectra shows the spacing between the two bands is ∼0.2 eV. The oscillator strengths increase according to the order f(**PE1-2**) < f(**PE1-3**) < f(**PE2-3**). The behavior of the fluorescence spectra mirrors that of the absorption spectra, with **PE1-2** blue-shifting from

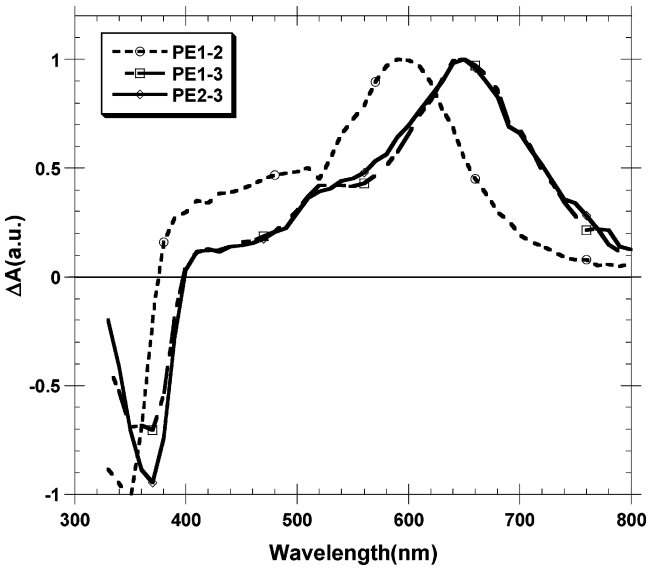

Figure 3. Triplet state absorption spectra obtained from excitation at 355 nm of a degassed benzene solution at room temperature.

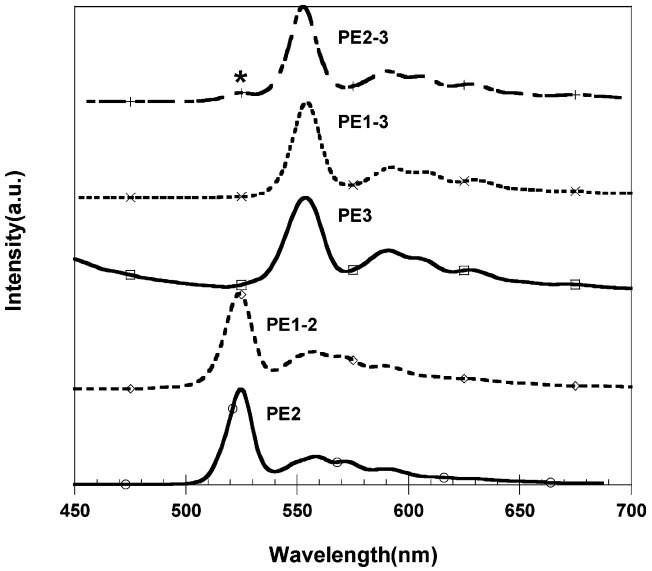

Figure 4. Phosphorescence spectra of chromophores dissolved in methyltetrahydrofuran glass at 77 K resulting from excitation at 350 nm. The peak marked with an asterisk is the weak emission from the **PE2** ligand of **PE2-3**.

PE1-3 and **PE2-3**, both of which have similar emission spectra. Unlike the absorption spectra, each of the emission spectra have only one band and do not show distinct vibronic structure.

The triplet state absorption spectra (Figure 3) are similar to ground state absorption and emission spectra. **PE1-2**'s spectrum is blue-shifted from those of **PE1-3** and **PE2-3**, which are nearly identical. All three spectra have a major band: 590 nm for **PE1-2** and 650 nm for **PE1-3** and **PE2-3** as well as a minor band: ~485 nm for **PE1-2** and 525 nm for **PE1-3** and **PE2-3**. The bleaching region shows **PE1-2** bleaching at ~350 nm, whereas **PE1-3** and **PE2-3** bleach at ~370 nm. The average energy difference between the two bands is ~0.4 eV. The triplet state lifetimes (Table 2) follow the trend τ(**PE1-2**) < τ(**PE1-3**) ~ τ(**PE2-3**).

We collected phosphorescence spectra of **PE1-2**, **PE1-3** and **PE2-3** and compared these spectra to phosphorescence from **PE2** and **PE3** (Figure 4). We find that the phosphorescence spectrum of **PE1-2** to be identical to that of **PE2**, and the spectrum of **PE1-3** and **PE2-3** to be identical to that of **PE3**.

TABLE 3: Summary of State Energies

compd	E_S[a,c]	E_T	ΔE_{ST}	E_{TT}
PE1-2	3.44	2.38	1.06	2.10
PE1-3	3.21	2.26	0.95	1.91
PE2-3	3.21	2.26	0.95	1.91
PE1[b]	3.58	2.82	0.76	1.97
PE2	3.29	2.38	0.91	2.14
PE3	3.21	2.26	0.95	1.94

[a] eV. [b] State energies for **PE1**, **PE2** and **PE3** were previously published. [c] E_S was measured from the intersection of the ground state absorption and fluorescence spectra and E_T from the blue edge of the phosphorescence spectrum.

TABLE 4: Various DFT Calculation Results

compd	E_{GS}[a]	E_{TS}[b]	E_T[c]	μ[d]	E_S[e]	f[f]	CI result
PE1	−987.2223	−987.1177	2.85	1.49	4.25	0.10	0.48(H → L)[7]
PE2	−1601.5540	−1601.4691	2.31	3.17	3.37	2.49	0.67(H → L)
PE3	−2215.8844	−2215.8046	2.17	5.05	2.96	3.88	0.65(H → L)
PE1−2	−1294.3882	−1294.3032	2.31	4.55	3.48	1.52	0.66(H → L)
PE1−3	−1601.5534	−1601.4737	2.17	6.86	3.03	2.08	0.67(H → L)
PE2−3	−1908.7192	−1908.6394	2.17	5.56	3.02	2.40	0.66(H → L)

[a] Ground state energy (*H*) calculated from optimized singlet state geometry. **PE1**, **PE2** and **PE3** are assumed to have C_{2h} symmetry. **PE1-2**, **PE1-3**, and **PE2-3** are assumed to have C_s symmetry. [b] Triplet state energy (*H*) calculated from optimized triplet state geometry. All chromophores are assumed to have C_1 symmetry. [c] E_T (eV) is the difference between triplet state energy and ground state energy. [d] Triplet state dipole moment (D). [e] Transition energy (eV) calculated from a TDDFT calculation. In **PE1**, the state shown is state 5. For all others, the state shown is state1. [f] Oscillator strength. [g] **PE1** also had 0.48 (H−1 → L+1).

In the **PE2-3** emission spectrum, we also observe a weak emission attributable to the 0−0 emission band from the **PE2** ligand. Table 2 summarizes data obtained from ground state absorption and emission spectra.

Table 3 lists all the state energies plus previously published state energy data for **PE1**, **PE2** and **PE3**.[1,11] The trend in state energies for E_S is **PE1** > **PE1-2** > **PE2** > **PE1-3** ~ **PE2-3** ~ **PE3**. The trend for the E_T state energy is **PE1** > **PE1-2** = **PE2** > **PE1-3** = **PE2-3** = **PE3**. With the exception of **PE1**, all ΔE_{ST} values are around 1 eV. The E_{TT} values follow the trend **PE1-2** ~ **PE2** > **PE1-3** ~ **PE2-3** ~ **PE3**.

Table 4 lists results of various calculations. Listed is the ground state energy after geometry optimization and the corresponding energy of the triplet-state-optimized geometry. As a test of our method, we did similar ΔSCF calculations for the monosubstituted **half-PE*n*** chromophores and compared them to experimental E_T values.[12] For the **half-PE*n*** compounds, we found the calculated (experimental) E_T values to be **half-PE1**: 2.88 (2.92); **half-PE2**: 2.32 (2.39); **half-PE3**: 2.17 (2.28). By calculating the difference between the two energies, we determine the E_T trend to be **half-PE1** ~ **PE1** > **half-PE2** = **PE2** = **PE1-2** > **half-PE3** = **PE1-3** = **PE2-3** = **PE3**. The calculated triplet state dipole moments follow the trend **PE1** < **PE2** < **PE1-2** < **PE3** < **PE2-3** < **PE1-3**. E_S is estimated from the lowest-lying allowed transition having oscillator strength greater than 0.1. The Supporting Information lists all the electronic states obtained from the TDDFT calculation. The next most intense state is about 0.3−0.4 eV higher in energy with 70−80% lower oscillator strength. The E_S values follow the trend **PE1** > **PE1-2** > **PE2** >**PE1-3** ~ **PE2-3** ~ **PE3**. The oscillator strengths order according to **PE1** < **PE1-2** < **PE1-3** < **PE2-3** < **PE2** < **PE3**. Examination of the configuration interaction (CI) coefficients show the largest configuration of this state is a highest occupied molecular orbital (HOMO) → lowest unoccupied molecular orbital (LUMO) transition.

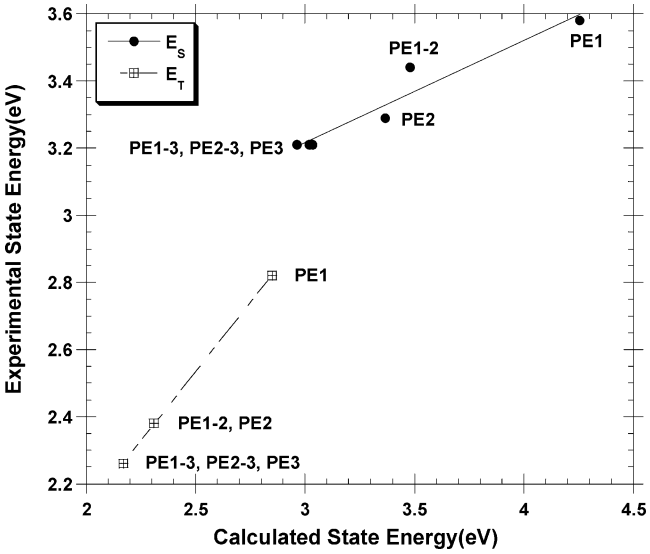

Figure 5. Comparison of calculated and experimental state energies. The triplet state energy E_T was calculated by the ΔSCF DFT method. The singlet state energy was calculated by the TDDFT method.

Figure 5 shows a plot of the calculated vs measured E_S and E_T values. A plot of E_T(experimental) vs E_T(calculated) have an excellent linear correlation. The linear fit gives the expression (in eV),

$$E_T(\text{expt})\ (\text{eV}) = 0.4758 + 0.8228E_T(\text{calc}) \quad r = 1$$

A similar plot for E_S gives the expression

$$E_S(\text{expt})\ (\text{eV}) = 2.3014 + 0.3048E_S(\text{calc}) \quad r = 0.9649$$

Although there is a lower correlation, the calculated E_S predicts the correct ordering of state energies with chromophore size.

Figure 6 shows images of the HOMO and LUMO for the chromophores. Neglecting the phosphines, **PE1**, **PE2** and **PE3** have D_{2h} symmetry. The HOMO consists of p orbitals on each of the phenylacetylene units and a d orbital on the platinum and has b_{2g} symmetry. The nodes cut through the bonds. Each phenylacetylene unit has two nodes, one through the phenyl group and one through the phenylacetylene carbon−carbon bond. There is another node between the platinum-carbon bond and a node between the lobes of the d orbital on the platinum atom. The LUMO consists of p orbitals on the phenylacetylene units and an empty d orbital on the platinum and has b_{3u} symmetry. The nodes cut through the bonds. Each phenylacetylene unit has three nodes, two in the phenyl group and one bisecting the acetylene group. There is another node bisecting the Pt−C bond and the Pt d orbital. An allowed HOMO → LUMO transition is the z-polarized B_{1u} state and is assigned as an ^1L_a state.[20−22] In **PE1**, there are 7 nodes in the HOMO, and 6 in the LUMO, showing the allowed optical transition follows the $\Delta q = \pm 1$ selection rule, as well as the g → u rule. The same analysis holds true for **PE2** and **PE3**.

If the phosphines in **PE1-2**, **PE1-3** and **PE2-3** are neglected, the chromophores have C_{2v} symmetry. Both B_{2g} and B_{3u} representations in D_{2h} transform as B_1 in C_{2v}. Similarly, both A_g and B_{1u} representations in D_{2h} transform as A_1 in C_{2v}. Like the **PE*n*** complexes, the HOMO consists of p orbitals on the phenylacetylene groups and a d orbital on the platinum and had b_1 symmetry. By looking at the "inversion" symmetry through the platinum atom, the p orbitals of corresponding atoms on opposite sides of the ligand have the same sign, giving them "g" symmetry. In **PE1-3** and **PE2-3** there is less electron density on the outer phenyl of the **PE3** ligand. The phenylacetylene node pattern is the same as seen in the **PE*n*** complexes. The LUMO consists of p orbitals on the phenylacetylene units and smaller contribution from the d orbital on the platinum atom and has b_1 symmetry. The "inversion" symmetry through the platinum atom shows the p orbitals of corresponding atoms on opposite sides of the ligand have opposite signs, giving them "u" symmetry. Because the d orbital has "g" symmetry, there is bonding between the platinum d orbital and one of the acetylene p orbitals. As in **PE*n***, each phenylacetylene unit has three nodes. An allowed HOMO → LUMO transition is a z-polarized A_1 state. In **PE1-2** the HOMO has 10 nodes, and the LUMO has 11 nodes, showing a $\Delta q = \pm 1$ selection rule. Analysis of the p orbital signs shows "g" → "u" character in the HOMO → LUMO transition. Similar analyses hold true in **PE1-3** and **PE2-3**.

Table 5 summarizes ground and triplet state geometry data for **PE2**. Complete geometry data for all the other chromophores are listed in Table S1 of the Supporting Information. In Table S1, a comparison of two chromophores **PEa-b** and **PEc-d**, shows that when **a** = **c**, the ground and triplet state geometries of the two left ligands are identical. When **b** = **d**, the ground and triplet state geometries of the two right ligands are identical. Table 5 shows ground and triplet state bond lengths for the right **PE2** ligand. The bond lengths for the left ligand triplet state are the same as the ground state. For a given number of phenylacetylene units in a ligand, the ground and triplet state geometries in both the left and right ligands are the same. The average ground state acetylene bond length, 1.23 Å, is close to the standard bond length of 1.20 Å. The bonds R_3, R_7 and R_9 have an average length of 1.43 Å, making them intermediate between a single bond (1.54 Å) and a double bond (1.36 Å). The average bond length in the phenyl rings is 1.41 Å, close to the standard length for a benzene carbon−carbon bond (1.39 Å). In the geometry optimizations, the **PE** ligand is constrained to be planar. A published X-ray structure of **PE2** gives R_2 = 1.214 Å and R_8 = 1.199 Å[4] vs our calculated values of 1.243 and 1.229 Å. Our calculated bond lengths are 0.03 Å larger than the experimental values, but there is good agreement for the difference between R_2 and R_8, 0.015 Å. In the triplet state there are only small geometry changes in the left ligand. In the right ligand, the acetylene bond lengths increase, whereas the adjoining carbon−carbon bonds decrease in length, giving the linkage more allene character. There are also decreases in the 2′−3′ bond lengths, while the 1′−2′ and 3′−4′ lengths increase. The net result of these changes give the ligand more quinone character. Table S1 also lists root mean square (rms) bond length changes in each of the phenylethynyl units of the right ligand as a function of position from the central platinum. The largest rms bond length changes occur in **PE1**, with smaller changes in larger ligands. In **PE3**, the largest geometry distortion occurs in the central phenylethynyl unit. To estimate ligand flexibility, we calculated the barrier to rotation about the phenylacetylene linkage in the **PE2-H** ligand to be 1.6 kcal/mol. The rotation barrier of the **PE2-H** ligand in the triplet state is estimated to be 9.4 kcal/mol. For each of the ligands, the electron affinity ($-E_{LUMO}$ in eV from optimized geometry) is calculated to be **PE1-H**: 0.78; **PE2-H**, 1.61; **PE3-H**, 1.92.

Figure 7 shows plots of the spin density of the triplet state. The chromophores are divided into the individual phenylacetylene units of either the left or right ligand, and the central platinum/phosphine units. With the exception of the platinum/phosphine unit of **PE1**, having a spin density of 0.20, there is

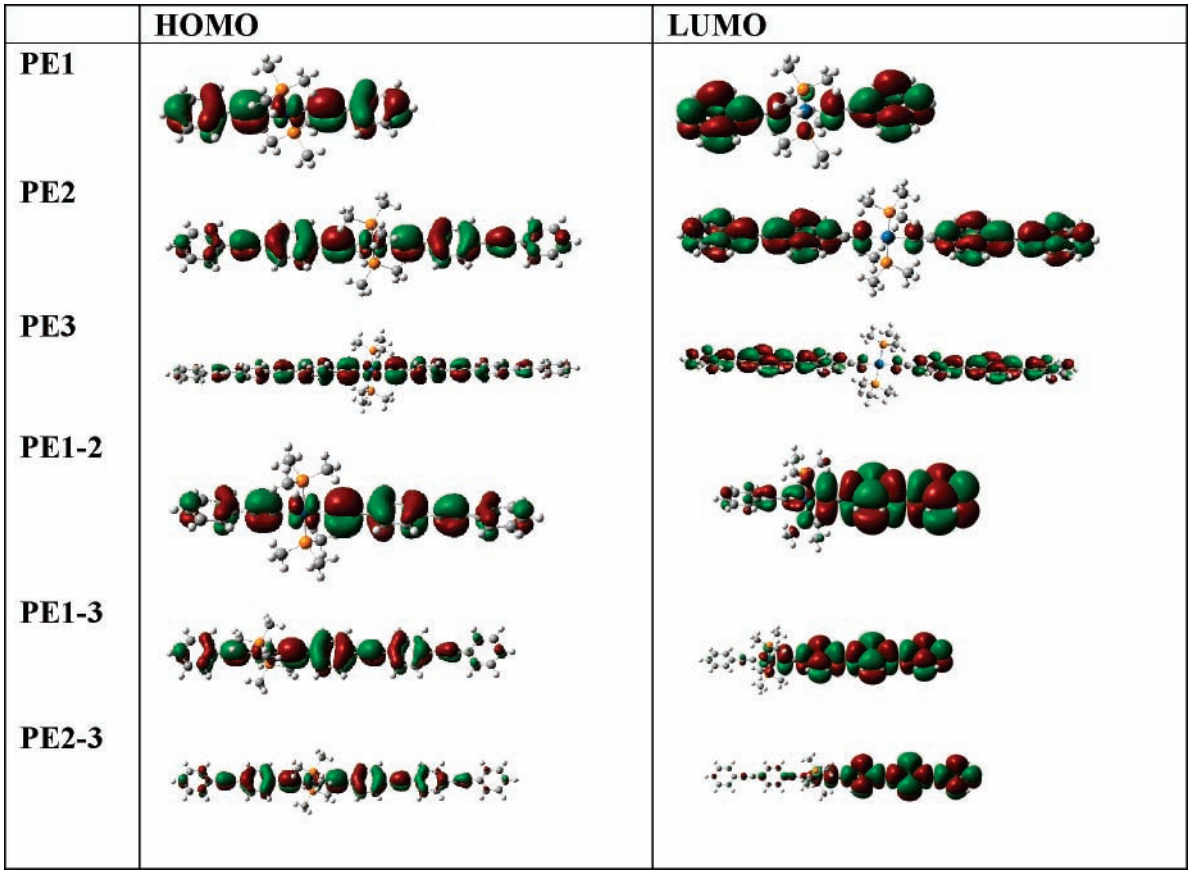

Figure 6. Frontier molecular orbitals of the various compounds obtained from DFT calculations of the geometry optimized structure.

TABLE 5: Bond Length Data for Ground State and Triplet State of PE2

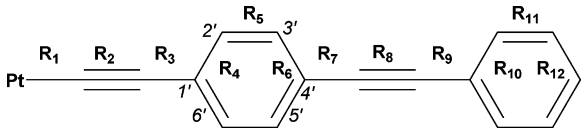

bond	**PE2**(S_0)[a]	**PE2**(T_1)	Δ[b]
R_1	2.014	1.993	−0.021
R_2	1.243	1.264	0.021
R_3	1.434	1.392	−0.042
R_4	1.423	1.464	0.041
R_5	1.399	1.370	−0.029
R_6	1.421	1.470	0.049
R_7	1.431	1.377	−0.054
R_8	1.229	1.255	0.026
R_9	1.433	1.405	−0.028
R_{10}	1.420	1.435	0.015
R_{11}	1.404	1.399	−0.005
R_{12}	1.409	1.415	0.006

no significant spin density on the platinum/phosphine unit. For all the compounds, the left ligand has virtually no spin density. Instead, most of the spin density is confined to the right ligand. In the asymmetric complexes, the triplet exciton is confined to the larger, lower energy ligand. The magnitude of the spin density is only a function of the right ligand size. The right ligand spin densities are identical in **PE1-2** and **PE2**. The spin densities of the right ligands of **PE1-3**, **PE2-3** and **PE3** are also identical. As the length of the right ligand increases from one to three phenylacetylene units, the spin density of the phenylacetylene nearest the platinum atom decreases from 1.70 to 0.25. The spin density of the second phenylacetylene unit increases from 0.59 to 0.95. The spin density on the third phenylacetylene unit is 0.73. The average spin density per

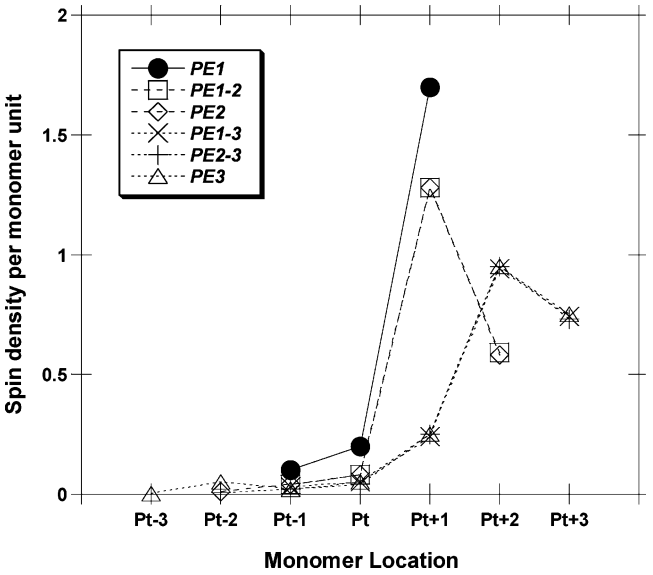

Figure 7. Spin densities obtained from DFT calculations of triplet state optimized geometry. The labels on the abscissa refer to monomer units. "Pt" refers to the central $Pt(PBu_3)_2$ group. Labels "Pt+1", "Pt+2" and "Pt+3" refer to successive phenylethynyl monomer units on the right ligand, with "Pt+1" being the phenylethynyl group bound to platinum. Similarly, "Pt-1", "Pt-2" and "Pt-3" refer to the left ligand, with "Pt-1" being the phenylethynyl group bound to the platinum. The ordinate refers the sum of atomic spin density of each phenylethynyl or $Pt(PBu_3)_2$ group.

functional group follows the trend Pt/phosphine, 0.086; ethynyl, 0.694 and phenyl, 1.22. As a comparison, a geometry optimization for the T_1 state of the butadiyne **PE1-BD** ($C_6H_5-C\equiv C-C\equiv C-C_6H_5$) shows the spin densities are symmetrically placed throughout the molecule, with the acetylene carbons having a

spin density of 1.064 and the phenyl groups having a spin density of 0.936.

Discussion

What is the relation between molecular structure and the delocalization of the singlet and triplet excitons? A theoretical and experimental investigation of the polymer poly(Pt(PBu$_3$)$_2$-(C≡CC$_6$H$_4$)) finds the T_1 exciton is localized on a single phenylene ring and the S_1 and T_n excitons are delocalized over several monomer units.[23] The spectra of a series of oligomers having the formula C$_6$H$_5$(C≡C−Pt(PBu$_3$)$_2$−C≡CC$_6$H$_4$)$_n$−H, $n = 1-5$, 7, show similar trends.[2] The ground state absorption and fluorescence spectra have systematic red shifts as the oligomer length increases. In contrast, the phosphorescence spectra have only small red shifts with increasing oligomer length. An investigation of the photophysics and photochemistry of platinum acetylide stilbenes also gives evidence that triplet state resides on one ligand.[24] Our group has done several studies on the relationship between platinum acetylide length and singlet state energy, including **PE*n***,[2] their analogous butadiynes,[11] the **half-PE*n*** complexes[12] and sydnone-containing complexes.[19] In all these studies the singlet state energy E_S decreases as the molecular length increases, whereas the triplet state energy E_T has less dependence on molecular length, supporting the idea that the triplet state is more localized than the singlet state.

The HOMO consists of π orbitals residing on the phenylacetylene units and 5d orbitals on the platinum. As shown in Table 1, the Pt−C carbon chemical shifts of the asymmetric complexes split into two values. The result suggests the Pt−C chemical shift is more strongly influenced by the carbon's own ligand environment rather than by the ligand across the platinum center. Examining Figure 6, the antibonding nature of the Pt−C bond increases the influence of the ligand on the Pt−C chemical shift and decreases the influence of the other ligand. The ^{13}C NMR data and DFT calculations on the asymmetric complexes give evidence of a ground state dipole moment. Polar asymmetric complexes have been described in the literature, where the asymmetrical complexes Pt(C≡CC$_6$H$_4$OCH$_3$)(C≡CC$_6$H$_4$NO$_2$)(PBu$_3$)$_2$ and (Pt(C≡CC$_6$H$_4$N-(CH$_3$)$_2$)(C≡CC$_6$H$_4$NO$_2$)(PBu$_3$)$_2$ have been shown to have dipole moments of 5 D.[25]

Our TDDFT calculations of the E_S values correlate well with the experimental values. There does appear to be a limit to the conjugation length, as the E_S values of **PE1-3**, **PE2-3** and **PE3** are about the same, a trend also seen in the TDDFT calculations. The CI coefficients depict the S_1 state as having predominantly HOMO → LUMO character. The LUMO consists of π^* orbitals on the ligands with the central d orbital empty. Inspection of the **PEa-b** LUMOs (Figure 6) reveals transfer of electron density from the left to the right ligand, giving them charge transfer (CT) character. From these results we conclude the S_1 state in **PEa-b** is a metal to ligand charge transfer (MLCT) with ligand-to-ligand CT character. A simple picture of the LUMO is a linear combination of excited ligand orbitals situated between an empty platinum d orbital.

$$^1\Psi^* = c_1\,{}^1\phi_a^* + c_2\,{}^1\phi_b^* \qquad (1)$$

In the symmetric **PE*n*** complexes, $c_1 = c_2 = 2^{-1/2}$. The LUMO of the asymmetric **PEab** chromophores has CT character, so $c_2 > c_1$. When the LUMO is only located on ligand **b**, $c_2 \sim 1$.

The phosphorescence spectra of the asymmetric complexes **PEa-b** are nearly identical to those of the symmetric complexes **PEb**, where **b** is the more conjugated ligand. Our DFT calculations give a strong correlation between calculated and experimental E_T values. The accuracy of our calculations agrees with previous theoretical work,[26] where DFT successfully calculates E_T within 0.1 eV of experiment.

A simple picture of the triplet state is a linear combination of localized triplet excitons.

$$^3\Psi^* = c_1\,{}^3\phi_a^*\,{}^1\phi_b + c_2\,{}^1\phi_a\,{}^3\phi_b^* \qquad (2)$$

The triplet exciton is confined to one ligand, and the other ligand is in the ground state. The triplet exciton migrates along a reaction coordinate describing ligand distortion, with the exciton migration potential energy surface having a double minimum.[14] During a phosphorescence experiment, emission of a photon occurs from the ligand carrying the exciton, and the spectrum gives no information about exciton migration, so the data are interpreted as describing "confinement". When the triplet energy difference between **a** and **b** is small, the chromophore behaves more like the symmetric **PE*n*** chromohores, with the exciton migrating between the two ligands. In symmetric **PE*n*** chromophores, the exciton has an equal probability of residing in either ligand, so $c_1 = c_2 = 2^{-1/2}$. In the asymmetric **PEa-b** chromophores, our experimental and computational results show the triplet exciton resides in the more conjugated, lower energy ligand, so $c_2 > c_1$. When the difference between the ligand energies is large, the exciton migration rate becomes small and the triplet exciton becomes confined to the lower energy ligand and $c_2 \sim 1$.

Does the distance between the ligands affect the localization of the triplet state? When electron exchange is small, energy transfer between the two ligands will occur by Forster transfer.[27] As electron exchange increases, energy transfer occurs by the Dexter mechanism. Very strong electron exchange causes the two ligands to behave as a single chromophore and our picture of localized triplet excitons migrating between the two ligands breaks down. As an example of this behavior, we did DFT calculations on **PE1-BD** and find the triplet state is symmetrically delocalized throughout the chromophore. The triplet state is then described by the following expression.

$$^3\Psi^* = c_1\,{}^3\phi_a^* + c_2\,{}^3\phi_b^* \qquad (3)$$

In the platinum complexes, the greater distance between the two ligands and the presence of the platinum center decreases their coupling. The triplet state can potentially reside on either ligand, having energies E_{T_a} and E_{T_b}. Intramolecular triplet energy transfer occurs between ligand **a** and ligand **b** via Dexter coupling, resulting in phosphorescence only from ligand **b**.[28] The average singlet−triplet splitting is 0.93 ± 0.10 eV in our compounds. Our calculated ΔE_{ST}, 1.02 ± 0.23 eV, is within 0.1 eV of the measured value but has a larger standard deviation. Our measured splitting contrasts to a ΔE_{ST} of 0.7 eV in polymeric platinum acetylide complexes.[3] The splitting energy is proportional to the overlap integral between the singlet and triplet excitons. Because the singlet state exciton resides in a chromophore than in the polymeric systems, it results in a larger energy gap.

Recent published data support our picture of the triplet state. A recently synthesized **PE1**−hexabenzocoronene shows a phosphorescence band at 578 nm from the hexabenzocoronene ligand and no emission from the **PE1** ligand.[29] Similar evidence of confinement of the triplet exciton to the core of a series of branched platinum acetylide complexes rather than the outer **PE1**-like ligands has been described.[30] All these results derive from Kasha's rule, where emission occurs from the lowest energy electronically excited-state of the molecule. This behavior

is observed in **PE1-2** and **PE1-3**, where the energy of ligand **1** is considerably higher than that of the other ligand. However, in **PE2-3**, we observe a small emission from ligand **2**. The LUMOs depicted in Figure 6 give evidence for the CT character of the excited states in the asymmetric complexes. In **PE1-2** and **PE1-3**, the difference in ligand electron affinity between ligand **1** and ligands **2** and **3**, calculated as 0.83 and 1.14 eV, respectively, is large enough that the triplet exciton resides only on ligands **2** or **3** ($c_2 \sim 1$). However, the difference in ligand electron affinity in **PE2-3**, 0.31 eV, is small enough that some measurable triplet exciton population of ligand **2** is possible ($c_1 > 0$). The measured energy difference between the 0−0 bands of the phosphorescence of ligands **2** and **3** is small enough (0.12 eV) that, during intersystem crossing, some of the excitation goes to ligand **2**. A similar result from the literature describes photoluminescence from a platinum acetylide polymer containing both phenyl and thiophene monomer units. Most of the emission comes from the lower energy thiophene units, but some emission is also observed from the higher energy phenyl units.[31] The study describes similar excited-state dynamics, where intersystem crossing results in the T_1 exciton residing on the phenyl unit with some phosphorescence from the phenyl, followed by energy transfer to the thiophene unit and subsequent phosphorescence from the thiophene unit.

In contrast to the behavior of the phosphorescence spectra, the $T_1 \rightarrow T_n$ spectrum red-shifts with increasing chromophore size.[1,11] A comparison of the $T_1 \rightarrow T_n$ transition energy of the **PE*n*** chromophores vs the monosubstituted **half-PE*n*** chromophores gives evidence this is an LMCT transition delocalized across the platinum center.[12] In the current work, the $T_1 \rightarrow T_n$ transition shows increased conjugation when **PE1-2** and **PE1-3** are compared, but the T_n state conjugation length of **PE2-3** is the same as that of **PE1-3**. The trend in triplet state lifetimes supports this idea, with the lifetimes of **PE1-3** and **PE2-3** being nearly equal. The conjugation length trends in the $T_1 \rightarrow T_n$ spectra mirror those seen in the ground state absorption and fluorescence spectra, showing the conjugation length of the T_n state changes in a similar manner as the S_1 and T_1 states.

The expression for the intersystem crossing rate constant can be used to analyze the factors underlying the conversion from the singlet to triplet state.[32,33]

$$k_{\mathrm{isc}} = k_{\mathrm{max}} \frac{\langle S_1|H_e|T_1\rangle^2}{\Delta E^2} \frac{\langle S_1|H_{\mathrm{so}}|T_1\rangle^2}{\Delta E^2} \langle \chi_{S_1}|\chi_{T_1}\rangle^2$$

This equation describes the interactions between S_1 and T_1 contributing to the rate of intersystem crossing. The first term describes electronic interactions. The second term describes spin−orbit coupling and the third term describes Franck−Condon factors.

Our experiments involve excitation of these chromophores initially in the ground state and observing the steady state and time-resolved behavior of the triplet state. We have previously shown the singlet state lifetime of these compounds is less than 30 ps and the intersystem crossing quantum yield is nearly unity.[1] Our calculations give good information about the S_0 state, the Franck−Condon S_1 state, and the T_1 state. We currently have no information about the S_1 and T_1 potential energy surfaces and the dynamics underlying the intersystem crossing process. Intersystem crossing occurs at geometries where the energy difference between the surfaces is small, and there is a strong electronic and vibrational interaction between the S_1 and T_1 states. These critical geometries may correspond to an avoided crossing minimum or a conical intersection between the S_1 and T_1 surfaces where a nonadiabatic transition will occur.[33−37]

A possible critical geometry is described by theoretical calculations of excited-state dynamics in phenylacetylene[38] and diphenylacetylene,[39,40] which suggest the formation of a stilbene-like biradicaloid S_1 state prior to the nonadiabatic jump to the T_1 state. This type of mechanism may occur in platinum acetylide complexes, where the initial D_{2h} symmetry Franck−Condon S_1 state relaxes to a biradicaloid state stilbene-like geometry, followed by conversion to the triplet state. Evidence for symmetry breaking during intersystem crossing has been obtained from a time-resolved infrared spectroscopy study of **PE1**, which shows a splitting of the Pt−C≡C stretch vibration into two peaks, suggesting the intersystem crossing mechanism, which includes symmetry breaking from the S_1 state having D_{2h} symmetry to the T_1 state having C_{2v} symmetry.[6] The authors of this paper propose the intersystem crossing process occurs by coupling of S_1 state B_{3u} symmetry PtC≡C antisymmetric stretch vibration to two uncoupled A_1 modes in the T_1 state. Similar spectroscopic behavior is observed in **PE2**, where a cumulated C=C=C stretch vibration appears in the T_1 state vibration spectrum.[13] Both of these experimental studies suggest, during intersystem crossing, conversion from aromatic ethynyl linkages to allene linkages occurs. The calculated bond length data given in Table 5 and Table S1 support this mechanism. The bonds undergoing greater than rms length change between the ground and triplet state in the right ligand are R_2 to R_4 in **PE1**, R_3 to R_7 in **PE1-2** and **PE2** and R_6, R_7, R_9 and R_{10} in **PE1-3**, **PE2-3** and **PE3**. All of these geometry changes involve the bonds connecting the phenyl groups. There are smaller distortions with the phenyl groups involving conversion from aromatic to quinone character. During intersystem crossing, the reaction coordinate for distortion of the molecule moves toward the critical geometry involved in the nonadiabatic transition between the singlet and triplet potential energy surfaces.[32] Does the symmetry-breaking process begin while the chromophore is still in the singlet state, or during the spin flip to the triplet state? Perhaps the relaxed singlet state is delocalized throughout the molecule, resulting from a Jahn−Teller distortion mechanism, leading to a geometry similar to the triplet state, promoting a nonadiabatic crossing to the triplet state. To understand these processes, it is necessary to monitor the rates of Franck−Condon S_1 state conversion to the relaxed S_1 state, followed by conversion to the triplet state, including possible possible population of both ligands, formation of stilbenoid intermediates and energy transfer to the lowest energy ligand. Future work will focus on the structure changes occurring on a subpicosecond time scale following excitation.[41]

Conclusions

We have synthesized the asymmetric complexes **PE1-2**, **PE1-3** and **PE2-3** and have determined various spectroscopic trends. The singlet state energy E_S decreases with increasing chromophore length, giving evidence that the singlet state is delocalized through the platinum. The DFT calculations suggest the S_1 state contains both intraligand CT and MLCT character. The triplet state energy E_T is a function of the longest ligand. The E_T trends suggest that the intersystem crossing mechanism involves movement of the triplet exciton to the lowest energy ligand. Our calculated E_T energies correlate well with the experimental values. The calculated triplet state geometry shows the geometry changes occur only on the lowest energy ligand. Spin density calculations also show the triplet state is confined to one ligand.

Acknowledgment. We thank Jean-Philippe Blaudeau, Gary Kedziora, and Kiet Nguyen for very helpful guidance in DFT calculations and Edward Lim for insightful discussions on the triplet state potential energy surface.

Supporting Information Available: Complete results of the TDDFT calculations, complete geometry and spin density data are available free of charge via the Internet at http://pubs.acs.org.

References and Notes

(1) Rogers, J. E.; Cooper, T. M.; Fleitz, P. A.; Glass, D. J.; McLean, D. G. *J. Phys. Chem. A* **2002**, *106*, 10108−10115.

(2) Liu, Y.; Jiang, S.; Glusac, K. D.; Powell, D. H.; Anderson, D. F.; Schanze, K. S. *J. Am. Chem. Soc.* **2002**, *124*, 12412−12413.

(3) Kohler, A.; Wilson, J. S.; Friend, R. H.; Al-Suti, M. K.; Khan, M. S.; Gerhard, A.; Bassler, H. *J. Chem. Phys.* **2002**, *116*, 9457−9463.

(4) Bruce, M. I.; Davy, J.; Hall, B. C.; Jansen van Galen, Y.; Skelton, B. W.; White, A. H. *Appl. Organomet. Chem.* **2002**, *16*, 559−568.

(5) Szafert, S.; Gladysz, J. A. *Chem. Rev.* **2003**, *103*, 4175−4205.

(6) Emmert, L. A.; Choi, W.; Marshall, J. A.; Yang, J.; Meyer, L. A.; Brozik, J. A. *J. Phys. Chem. A* **2003**, *107*, 11340−11346.

(7) Yam, V. W.-W. *Acc. Chem. Res.* **2002**, *35*, 555−563.

(8) Cooper, T. M.; Hall, B. C.; Burke, A. R.; Rogers, J. E.; McLean, D. G.; Slagle, J. E.; Fleitz, P. A. *Chem. Mater.* **2004**, *16*, 3215−3217.

(9) Cooper, T. M. *Encyclopedia of Nanomaterials and Nanotechnology*; Nalwa, H. S., Ed.; American Scientific Publishers: Stevenson Ranch, CA, 2004; Vol. 10, pp 447−470.

(10) Cooper, T. M.; McLean, D. G.; Rogers, J. E. *Chem. Phys. Lett.* **2001**, *349*, 31−36.

(11) Rogers, J. E.; Hall, B. C.; Hufnagle, D. C.; Slagle, J. E.; Ault, A. P.; McLean, D. G.; Fleitz, P. A.; Cooper, T. M. *J. Chem. Phys.* **2005**, *122*, 214708−214715.

(12) Cooper, T. M.; Krein, D. M.; Burke, A. R.; McLean, D. G.; Rogers, J. E.; Slagle, J. E. *J. Phys. Chem. A* **2006**, *110*, 4369−4375.

(13) Cooper, T. M.; Blaudeau, J.-P.; Hall, B. C.; Rogers, J. E.; McLean, D. G.; Liu, Y.; Toscano, J. P. *Chem. Phys. Lett.* **2004**, *400*, 239−244.

(14) Batista, E. R.; Martin, R. L. *J. Phys. Chem. A* **2005**, *109*, 9856−9859.

(15) Frisch, M. J.; Trucks, G. W.; Schlegel, H. B.; Scuseria, G. E.; Robb, M. A.; Cheeseman, J. R.; Montgomery, J. A.; Vreven, T.; Kudin, K. N.; Burant, J. C.; Millam, J. M.; Iyengar, S. S.; Tomasi, J.; Barone, V.; Mennucci, M.; Cossi, G.; Scalmani, G.; Rega, N.; Petersson, A. S.; Nakatsuji, H.; Hada, M.; Ehara, M.; Toyota, K.; Fukuda, R.; Hasegawa, J.; Ishida, M.; Nakajima, T.; Honda, Y.; Kitao, O.; Nakai, H.; Klene, M.; Li, X.; Knox, J. E.; Hratchian, H. P.; Cross, J. B.; Adamo, C.; Jaramillo, J.; Gomperts, R.; Stratmann, R. E.; Yazyev, O.; Austin, A. J.; Cammi, R.; Pomelli, C.; Ochterski, J. W.; Ayalo, P. Y.; Morokuma, K.; Voth, G. A.; Salvador, P.; Dannenberg, J. J.; Zakrewski, V. G.; Dapprich, S.; Daniels, A. D.; Strain, M. C.; Farkas, O.; Malick, D. K.; Rabuck, A. D.; Raghavachari, K.; Foresman, J. B.; Ortiz, J. V.; Cui, Q.; Baboul, A. G.; Clifford, S.; Cioslowski, J.; Stefanov, B. B.; Liu, G.; Liashenko, A.; Piskorz, P.; Komaromi, I.; Martin, R. L.; Fox, D. J.; Keith, T.; Al-Laham, M. A.; Peng, C. Y.; Nanayakkara, A.; Challacombe, M.; Gill, P. M. W.; Johnson, B.; Chen, W.; Wong, M. W.; Gonzaez, C.; Pople, J. A. *Gaussian 03W*, revision D.01; Gaussian, Inc.: Pittsburgh, PA, 2004.

(16) Norman, P.; Cronstrand, P.; Ericsson, J. *Chem. Phys.* **2002**, *285*, 202−220.

(17) Baev, A.; Rubio-Pons, O.; Gel'Mukanov, F.; Agren, H. *J. Phys. Chem. A* **2004**, *108*, 7406−7416.

(18) Koch, W.; Holthausen, M. C. *A Chemist's Guide to Density Functional Theory*; Wiley-VCH: Weinheim, 2001.

(19) Cooper, T. M.; Hall, B. C.; McLean, D. G.; Rogers, J. E.; Burke, A. R.; Turnbull, K.; Weisner, A. J.; Fratini, A.; Liu, Y.; Schanze, K. S. *J. Phys. Chem. A* **2005**, *109*, 999−1007.

(20) Platt, J. R., *J. Chem. Phys.* **1949**, *17*, 470−481.

(21) Serrano-Andres, L.; Merchan, M.; Jablonski, M. *J. Chem. Phys.* **2003**, *119*, 4294−4303.

(22) Amatatsu, Y.; Hasebe, Y. *J. Phys. Chem. A* **2003**, *107*, 11169−11173.

(23) Beljonne, D.; Wittman, H. F.; Kohler, A.; S., G.; Younus, M.; Lewis, J.; Raithby, P. R.; Khan, M. S.; Friend, R. H.; Bredas, J. L. *J. Chem. Phys.* **1996**, *105*, 3868−3877.

(24) Haskins-Glusac, K.; Ghiviriga, I.; Abboud, K. A.; Schanze, K. S. *J. Phys. Chem. B* **2004**, *108*, 4969−4978.

(25) Nguyen, P.; Lesley, G.; Marder, T. B.; Ledoux, I.; Zyss, J. *Chem. Mater.* **1997**, *9*, 406−408.

(26) Nguyen, K. A.; Kennel, J.; Pachter, R. *J. Chem. Phys.* **2002**, *117*, 7128−7136.

(27) Gonzalez, C.; Lim, E. C. *Chem. Phys. Lett.* **2000**, *322*, 282−288.

(28) Tian, H.; Yang, S. *J. Photochem. Photobiol. C: Photochem. Rev.* **2002**, *3*, 67−76.

(29) Kim, K.-Y.; Liu, S.; Kose, M. E.; Schanze, K. S. *Inorg. Chem.* **2006**, *49*, 2509−2519.

(30) Tao, C.-H.; Zhu, N.; Yam, V. W.-W. *Chem. Eur. J.* **2005**, *11*, 1647−1657.

(31) Schanze, K. S.; Silverman, E. E.; Zhao, X. *J. Phys. Chem. B* **2005**, *109*, 18451−18459.

(32) Turro, N. J. *Modern Molecular Photochemistry*; University Science Books: Sausalito, CA, 1991.

(33) Freed, K. F. *Acc. Chem. Res.* **1978**, *11*, 74−80.

(34) Dauben, W. G.; Salem, L.; Turro, N. J. *Acc. Chem. Res.* **1975**, *8*, 41−54.

(35) Salem, L.; Leforestiew, C.; Segal, G.; Wetmore, R. *J. Am. Chem. Soc.* **1975**, *97*, 479−487.

(36) Yarkony, D. R. *J. Phys. Chem. A* **2001**, *105*, 6277−6293.

(37) Worth, G. A.; Cederbaum, L. S. *Annu. Rev. Phys. Chem.* **2004**, *55*, 127−158.

(38) Amatatsu, Y. *J. Phys. Chem. A* **2006**, *110*, 4479−4486.

(39) Zgierski, M. Z.; Lim, E. C. *Chem. Phys. Lett.* **2004**, *387*, 352−355.

(40) Amatatsu, Y.; Hosokawa, M. *J. Phys. Chem. A* **2004**, *108*, 10238−10244.

(41) Srinivasan, R.; Feenstra, J. S.; Park, S. T.; Xu, S.; Zewail, A. H. *Science* **2005**, *307*, 558−563.